L-shell ionization studies of Pb and Bi with α particles

B. B. Dhal, T. Nandi, and H. C. Padhi
Institute of Physics, Bhubaneswar 751005, India
(Received 3 June 1993)

Ionization cross sections for the L subshells of Pb and Bi by α-particle bombardment (2.2–8.2 MeV) have been determined from the experimental data and the currently available radiative transition probabilities, fluorescence yields, and Coster-Kronig factors. The measured ionization cross sections and their ratios are compared with the results of ECPSSR calculations [ECPSSR denotes perturbed-stationary-state (PSS) theory with energy-loss (E), Coulomb deflection (C), and relativistic (R) corrections]. The measured individual cross sections for L_1 and L_2 subshells deviated in opposite directions from the theory, whereas their sum shows good agreement. The L_3 and total ionization cross sections obtained from the data also show good agreement with the ECPSSR theory. The ionization cross-section ratios $\sigma_{L_1}/\sigma_{L_2}$ and $\sigma_{L_3}/\sigma_{L_2}$ show large deviations from the ECPSSR theory. The experimental x-ray production cross-section ratios are found to be in better agreement with the theoretical results obtained from using ECPSSR ionization cross sections and the decay yield data of Xu and Xu [J. Phys. B **25**, 695 (1992)] rather than those obtained from using the decay yield data of Krause [J. Phys. Chem. Ref. Data **8**, 307 (1979)]. The x-ray production cross sections, however, are in better agreement with the theoretical results obtained from using the decay yield data of Krause. The measured centroid energy of the $L\gamma$ lines of Pb shows large deviations at high projectile energy, whereas for Bi large deviations are found at the low-energy region.

PACS number(s): 32.80.Cy, 32.80.Hd

I. INTRODUCTION

In an earlier paper [1] we presented our results on L-shell ionization studies of Pb and Bi for proton bombardment and in this work we present the results for α-particle bombardment in the energy range of 0.5–2.0 MeV/amu. Although considerable efforts have been put into understanding the L-subshell ionization process [2–6] by heavily charged particles, the situation still seems to be very fuzzy. The first study in Au for proton- and α-particle bombardment was reported by Datz *et al.* [2] which showed a significant deviation of the α-particle data from the proton data at low energy. It also indicated deviations for L_1-subshell ionization cross sections and the cross-section ratios $\sigma_{L_1}/\sigma_{L_2}$ and $\sigma_{L_3}/\sigma_{L_2}$ from both nonrelativistic and relativistic plane-wave Born approximation (PWBA) theories [7]. After this work Chang *et al.* [3,4] reported their work on L-subshell ionization for various heavy elements by α-particle bombardment in which they showed for the first time that the low-energy behavior of the cross-section ratio $\sigma_{L_3}/\sigma_{L_2}$ is dependent on the outer electronic configuration of the target atom. However, their conclusion was refuted by the work of Li, Clark, and Greenlees [5], which did not show any target outer electronic configuration dependence for the behavior of $\sigma_{L_3}/\sigma_{L_2}$ ratio at low projectile energy. In the theoretical work of Sarkadi and Mukoyama [8,9] it was shown that for heavily charged particle bombardment ($Z>2$) the experimental L_2-subshell ionization cross section deviates by almost one order of magnitude from the relativistic plane-wave Born approximation– with binding energy and Coulomb deflection correction (RPWBA-BC) theory. This anomalous behavior was shown to be arising from collision-induced transitions of a vacancy between the L subshells. The large L_2-subshell ionization anomally was later theoretically accounted by Sarkadi and Mukoyama [10] by taking the subshell coupling effects into account. Recently, Xu and Xu have made the calculation on relative and total L x-ray production cross sections of Bi for α-particle bombardment using their own decay yield data [11] and ECPSSR [ECPSSR denotes perturbed-stationary-state (PSS) theory with energy-loss (E), Coulomb deflection, (C), and relativistic (R) corrections] ionization cross sections [12,13] and showed that their results are in good agreement with the experimental results [3,6,14–16] for the total x-ray production cross section for the α-particle energy range 1.0–4.0 MeV. Looking at the reported results of L-subshell ionization of heavy elements one does not see a clear-cut picture on the position of various ionization theories *vis a vis* the experimental results. The present study was aimed at obtaining various physical quantities such as x-ray production cross sections, ionization cross sections, relative L x-ray intensities, and L-subshell ionization cross-section ratios from the data and compared with the existing theoretical calculations, so that one can get a better understanding of the L-subshell ionization process by the bombardment of heavily charged particles.

II. EXPERIMENTAL TECHNIQUE

The L x-ray spectra of Pb and Bi have been measured for α-particle bombardment at different energies. High pure ($\sim$99.9%) samples were used for the preparation of

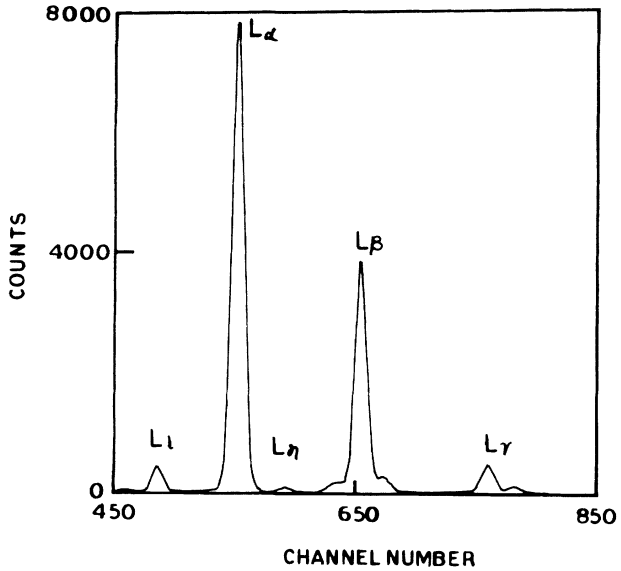

FIG. 1. A typical L x-ray spectrum of Pb at an α-particle energy of 6 MeV.

the targets. Thin (40 μg/cm^2) targets of Pb and Bi were prepared by vacuum evaporation onto aluminized Mylar films of thickness 1.75 mg/cm^2. The targets were bombarded by α particles with an energy of 2.28–8.18 MeV obtained from the 3-MV tandem pelletron accelerator at the Institute of Physics, India. To obtain the Li ($i=l$, α, β, γ, etc.) x-ray production cross sections from the measured x-ray yields, simultaneous x-ray and elastically scattered charged particle detection techniques were employed. Details of the experimental arrangement are described elsewhere [1]. The collimated α-particle beam of 1.5-mm diameter was directed onto the target which was kept tilted at 45° to the beam direction. The emitted L x-rays passed through a 3.5-mg/cm^2 Mylar chamber window, 5-cm air gap, and 0.012-mm-thick beryllium window before reaching the Si(Li) detector with an energy resolution of 170 eV full width at half maximum at 5.9 keV. The detector was placed 90° to the beam direction. The solid angles of both the silicon surface barrier and Si(Li) detectors have been well defined by placing suitable apertures in front of the detectors. Another advantage of the aperture was that it allowed the radiation to fall on the center of the active area of the detector. A typical x-ray spectrum of Pb at 6-MeV α-particle energy is shown in Fig. 1.

III. DATA ANALYSIS AND RESULTS

A. Data analysis

From the measured x-ray yields the Li x-ray production cross sections were estimated using the following relation:

$$\sigma_{Li}^{x}=\frac{4\pi Y_x^i \sigma_R(\theta)\Delta\Omega_p}{\epsilon_a \epsilon_d Y_R \Delta\Omega_x}\left[\frac{t_x}{t_R}\right], \tag{1}$$

where σ_{Li}^{x} is the x-ray production cross section (the index i refers to a particular component of L x-ray such as l, α, β, γ, etc.) of the Li component of the L x-ray spectrum, Y_x^i is the measured x-ray yield for the Li component, $\sigma_R(\theta)$ is the differential Rutherford scattering cross section, Y_R is the measured Rutherford yield, ϵ_d is the Si(Li) detector intrinsic efficiency, ϵ_a is the absorption correction for the Mylar chamber window and air path, $\Delta\Omega_p$ is the solid angle subtended by the charged particle silicon surface barrier detector, $\Delta\Omega_x$ is the solid angle subtended by the Si(Li) x-ray detector, t_x is the dead time correction for x-ray counting, and t_R is the dead time correction for charged particle counting.

The intrinsic efficiency of the Si(Li) detector was theoretically calculated using the following expression:

$$\epsilon_d(E)=e^{-(\mu_{\mathrm{Be}}x_{\mathrm{Be}}+\mu_{\mathrm{Au}}x_{\mathrm{Au}}+\mu_{\mathrm{Si}}\Delta x_{\mathrm{Si}})}(1-e^{-\mu_{\mathrm{Si}}x_{\mathrm{Si}}}) \tag{2}$$

where the μ's are the absorption coefficients due to the Be window of the detector, the gold layer on the Si(Li) crystal and Si(Li) crystal at the x-ray energy E, and Δx_{Si} is the thickness of the insensitive region of the Si(Li) crystal. The x's are as per the specifications of the detector manufacturer and the absorption coefficients are taken from the table of Hubbell *et al.* [17]. Y_x^i and Y_R^i are obtained from the measured x-ray and Rutherford spectra, respectively. The x-ray yields for the various L x-ray components were estimated by the least-squares peak fitting program and the Rutherford yields were calculated by summing the counts under the elastic peak. Corrections due to absorption in the Mylar chamber window and air path were applied in the usual manner. Correction due to self-absorption in the sample was found to be negligible.

In order to interpret the measured x-ray production cross sections we tried to evaluate (1) the experimental subshell ionization cross sections and their ratios and then compare them with theory, and (2) compare the measured x-ray production cross-section ratios with the theoretical results obtained from theoretical ionization cross sections and the presently available different sets of decay yield data. For getting the experimental ionization cross sections from the measured production cross sections one runs through the following analytic formulas relating x-ray production cross sections to the ionization cross sections:

$$\sigma_{Ll}^{x}=(\sigma_{L_1}f_{13}+\sigma_{L_1}f_{12}f_{23}+\sigma_{L_2}f_{23}+\sigma_{L_3})\omega_3 F_{3l}\ , \tag{3a}$$

$$\sigma_{L\alpha}^{x}=(\sigma_{L_1}f_{13}+\sigma_{L_1}f_{12}f_{23}+\sigma_{L_2}f_{23}+\sigma_{L_3})\omega_3 F_{3\alpha}\ , \tag{3b}$$

$$\sigma_{L\beta}^{x}=\sigma_{L_1}\omega_1 F_{1\beta}+(\sigma_{L_1}f_{12}+\sigma_{L_2})\omega_2 F_{2\beta}+(\sigma_{L_1}f_{13}+\sigma_{L_1}f_{12}f_{23}+\sigma_{L_2}f_{23}+\sigma_{L_3})\omega_3 F_{3\beta}\ , \tag{3c}$$

$$\sigma_{L\gamma}^{x}=\sigma_{L_1}\omega_1 F_{1\gamma}+(\sigma_{L_1}f_{12}+\sigma_{L_2})\omega_2 F_{2\gamma}\ , \tag{3d}$$

where σ_{Ll}^{x}, $\sigma_{L\alpha}^{x}$, $\sigma_{L\beta}^{x}$, and $\sigma_{L\gamma}^{x}$ are the x-ray production cross sections of the components of Ll, $L\alpha$, $L\beta$, and $L\gamma$, respectively. σ_{L_1}, σ_{L_2}, and σ_{L_3} are ionization cross sec-

tions of the subshells L_1, L_2, and L_3, respectively, and ω_1, ω_2, and ω_3 are the corresponding subshell fluorescence yields. F_{ny} (F_{3l}, $F_{3\alpha}$, etc.) are the fraction of the radiative widths of the subshell L_n (L_1,L_2,L_3) contained in the yth spectral line, i.e.,

$$F_{ny}=\Gamma_{ny}/\Gamma_n \tag{4}$$

(for example, $F_{3l}=\Gamma_{3l}/\Gamma_3$) where Γ_n is the total linewidth of L_n. The parameters f_{12}, f_{23}, and f_{13} are the Coster-Kronig transition probabilities for $L_1\rightarrow L_2$, $L_2\rightarrow L_3$, and $L_1\rightarrow L_3$, respectively (the arrow indicates the direction of the electron vacancy transition between subshells).

The composite $L\gamma$ peak has been computer analyzed into four Gaussians whose χ^2 value was found to be close to one for all projectile energies. Four components of $L\gamma$ were obtained; $L\gamma_5$ and $L\gamma_1$ which are related to the L_2 subshell and $L\gamma_{2+3}$ and $L\gamma_4$, which are related to the L_1 subshell. Examples, of this fitting for Pb and Bi at one projectile energy are presented in Fig. 2. Equation (3d) can be broken into

$$\sigma^x_{L\gamma_{2+3}}+\sigma^x_{L\gamma_4}=\sigma_{L_1}\omega_1 F_{1\gamma_{2+3+4}} \tag{5}$$

and

$$\sigma^x_{L\gamma_5}+\sigma^x_{L\gamma_1}=(\sigma_{L_1}f_{12}+\sigma_{L_2})\omega_2 F_{2\gamma_{5+1}}\ . \tag{6}$$

Equations (3d) and (6) can be solved iteratively for σ_{L_1} and σ_{L_2} by first ignoring f_{12} in Eqs. (6) and (3d). σ_{L_3} was obtained through Eq. (3b) by using the deduced σ_{L_1} and σ_{L_2} and the measured x-ray production cross-section $\sigma^x_{L\alpha}$. After this a consistency check was made for the $L\beta$ group through the comparison between the measured $\sigma^x_{L\beta}$ and that calculated from Eq. (3c). The average difference between the calculated and measured $\sigma^x_{L\beta}$ was found to be 3.0%–4.0% for the entire energy range.

B. Atomic parameters

The measured x-ray production cross sections are converted into ionization cross sections by using two sets of fluorescence yield data, one by Krause [18] and the other by Xu and Xu [11]. The fractional radiative widths used here are taken from the radiative emission rates calculated by Scofield [19]. The atomic parameters used in the present work are given in Table I.

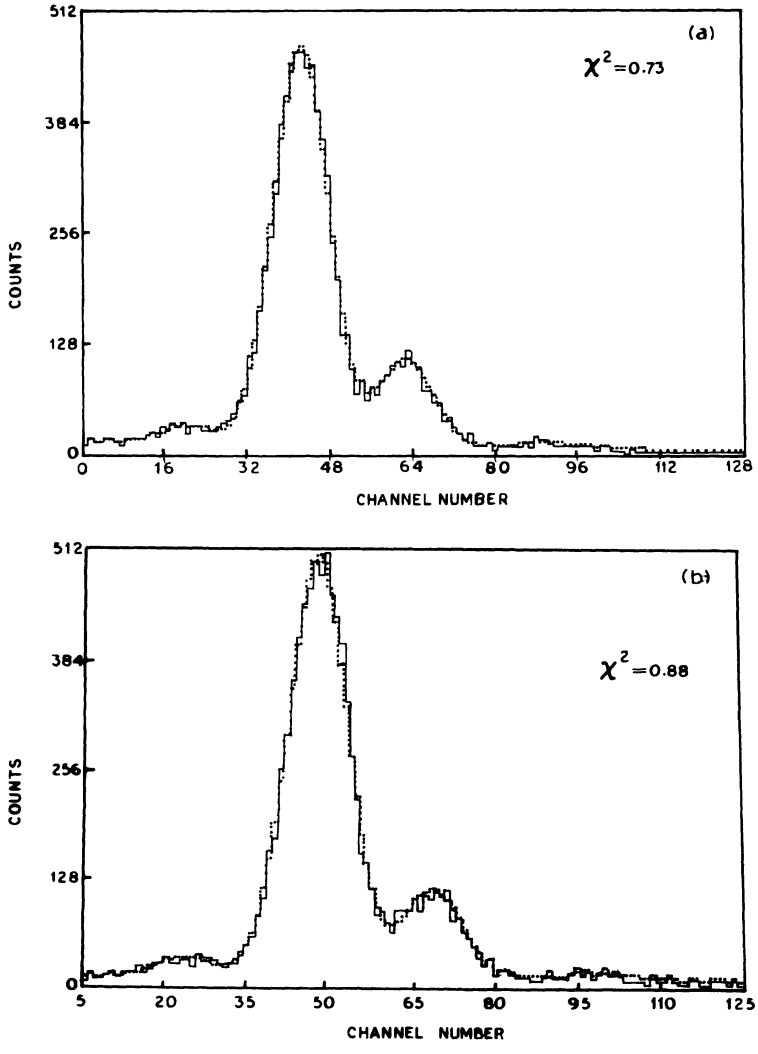

FIG. 2. Gaussian fits to the $L\gamma$ x-ray spectra of (a) Pb and (b) Bi. The χ^2 values of the fits are indicated.

TABLE I. L-subshell fluorescence and Coster-Kronig yields of Pb and Bi.

Target atom	Decay yield data set	ω_1	ω_2	ω_3	f_{12}	f_{13}	f_{23}
Pb	Krause [18]	0.112	0.373	0.360	0.12	0.58	0.116
	Xu and Xu [11]	0.135	0.405	0.326	0.040	0.661	0.091
Bi	Krause [18]	0.117	0.387	0.373	0.11	0.58	0.113
	Xu and Xu [11]	0.138	0.428	0.340	0.055	0.700	0.12

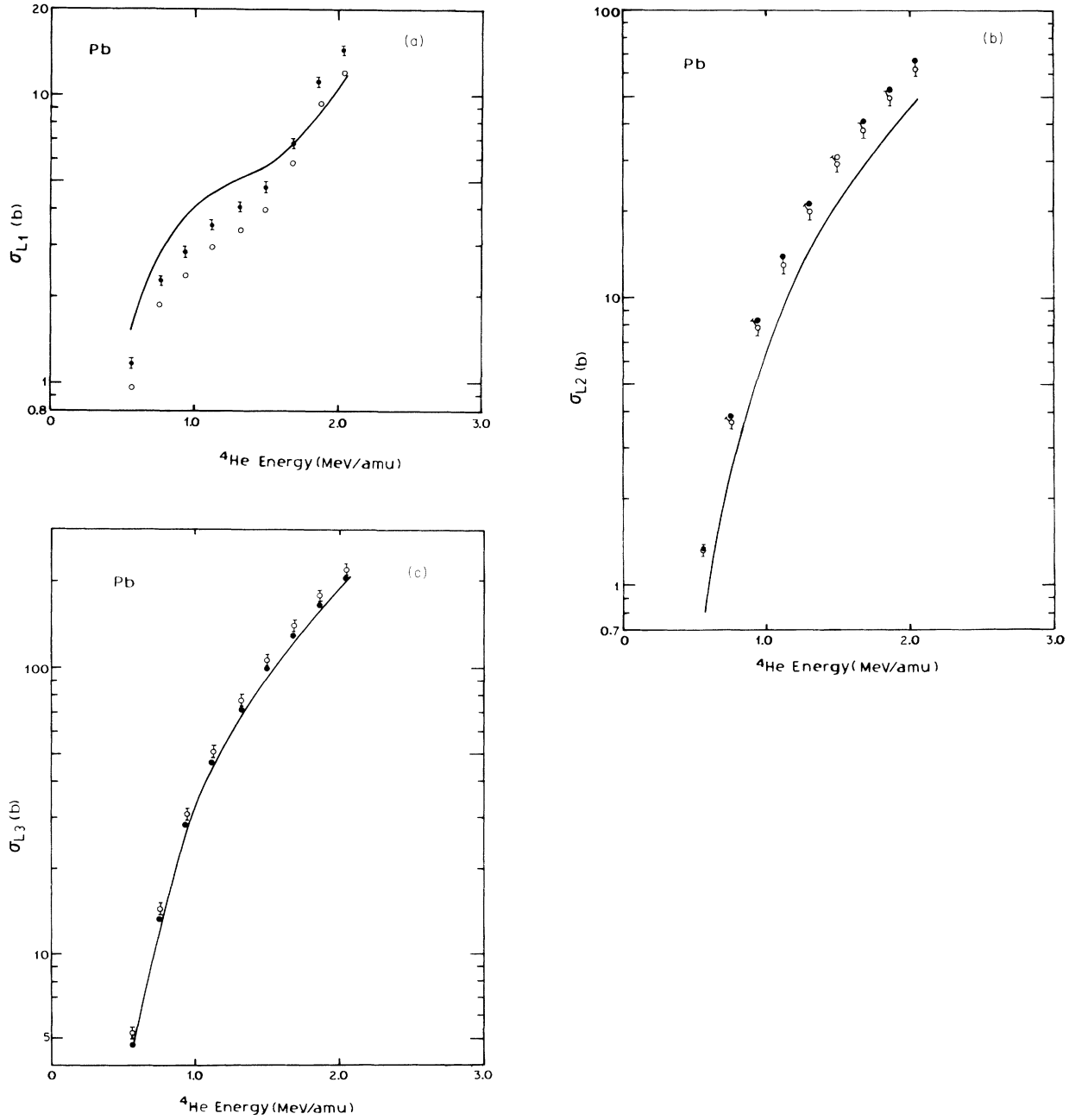

FIG. 3. L-shell ionization cross-sections of Pb for α-particle bombardment: (a) L_1 subshell, (b) L_2 subshell, (c) L_3 subshell: (——) corresponds to the ECPSSR theory; (○) corresponds to present experimental results obtained using the decay yield data of Xu and Xu; (●) corresponds to present experimental results obtained using the decay yield data of Krause.

C. Results and error analysis

The ionization cross sections σ_{L_1}, σ_{L_2}, and σ_{L_3} for Pb and Bi, obtained as described before, are shown in Figs. 3 and 4 together with the two theoretical results which will be discussed below. Previous experimental results for Bi [4,14,15] could not be plotted in Fig. 4 because of nonavailability of their data in tabulated form.

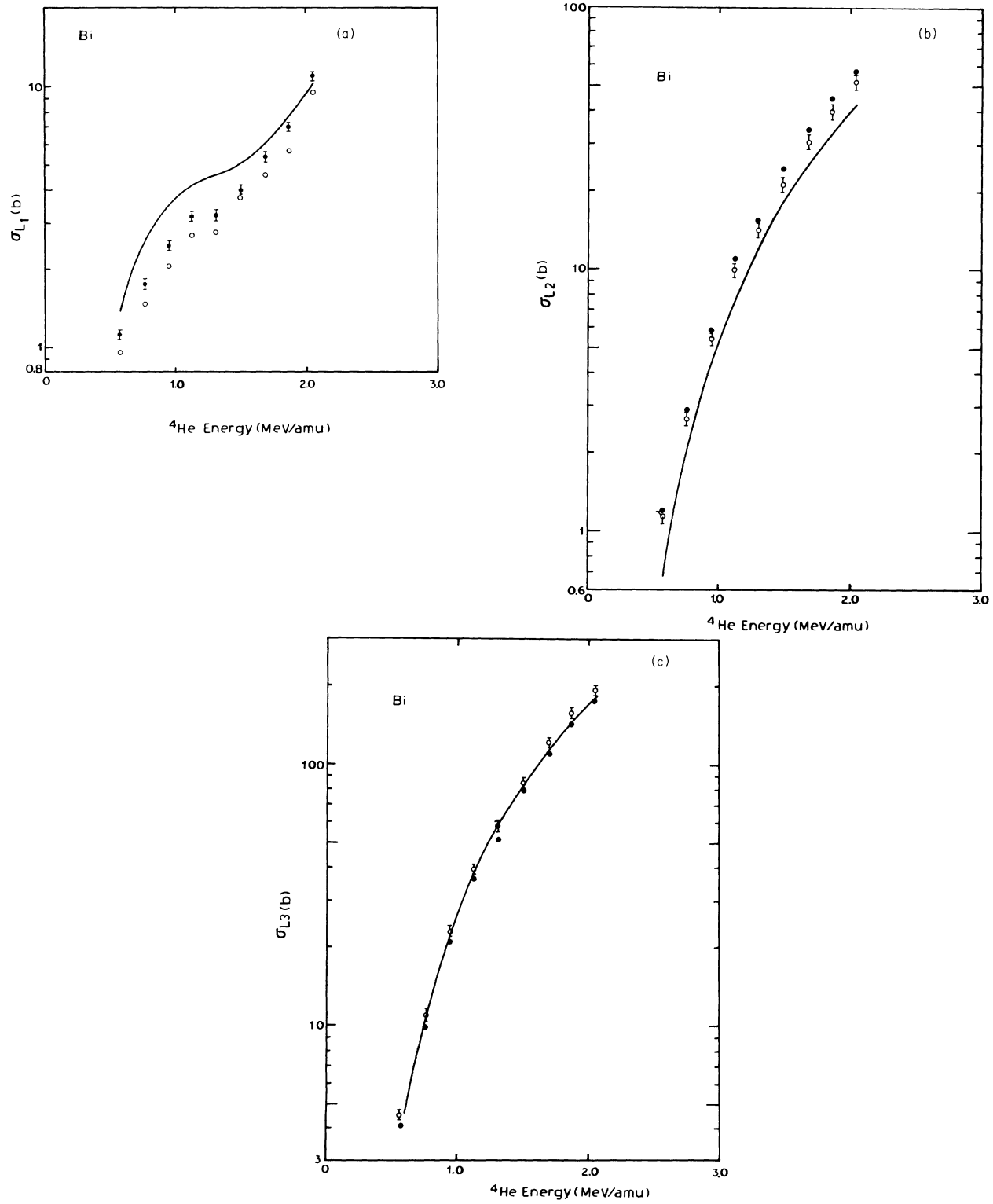

FIG. 4. L-shell ionization cross sections of Bi for α-particle bombardment: (a) L_1 subshell, (b) L_2 subshell, (c) L_3 subshell: (——) corresponds to the ECPSSR theory; (○) corresponds to present experimental results obtained using the decay yield data of Xu and Xu; (●) corresponds to present experimental results obtained from the data using the decay yield data of Krause.

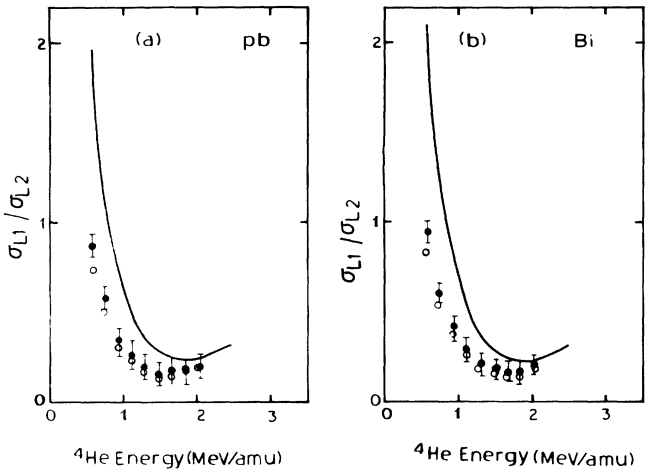

FIG. 5. Values of the ionization cross section ratio $\sigma_{L_1}/\sigma_{L_2}$ of (a) Pb and (b) Bi: (——) corresponds to the ECPSSR theory. (●) are obtained using Krause's decay yield data, and (○) are obtained using Xu and Xu's decay yield data.

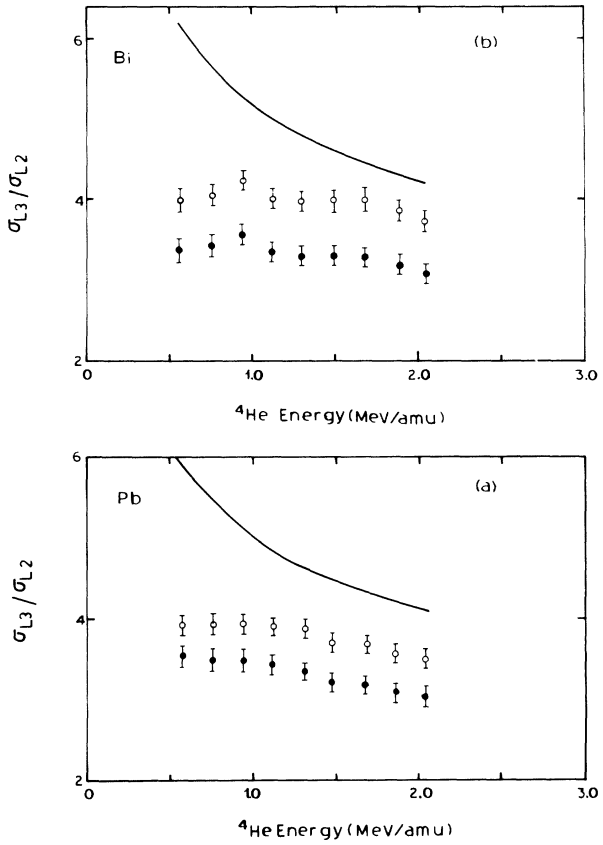

FIG. 6. Values of ionization cross-section ratio $\sigma_{L_3}/\sigma_{L_2}$ of (a) Pb and (b) Bi: (——) corresponds to the ECPSSR theory, (●) are obtained using the decay yield data of Krause, and (○) are obtained using the decay yield data of Xu and Xu.

The standard counting error for the $L\alpha$ x rays was 0.5%, $L\beta$ x rays 0.7% and $L\gamma$ x rays which relate to L_1 and L_2-subshell ionization was on the average less than 5%. In addition to this the other sources of experimental uncertainty come from the detector efficiency and absorption correction due to the Mylar chamber window and airpath. They contribute together an overall error of about 2.0%. The self-absorption in the target was negligible. Uncertainty in the estimation of the solid angles will be within 5.0%.

In the conversion process to ionization cross sections from x-ray yields, uncertainties in the atomic parameters, such as fluorescence yield, radiative transition rates, and Coster-Kronig transition probabilities may increase the uncertainty for the final absolute ionization cross sections. The error from this source could amount to about 10%. The error in the ratio of ionization cross sections $\sigma_{L_1}/\sigma_{L_2}$, $\sigma_{L_3}/\sigma_{L_2}$ will mainly be from counting error.

IV. DISCUSSION

The ionization cross sections of Pb and Bi which are plotted in Figs. 3 and 4 show deviations in opposite directions from the ECPSSR theory [12,13] for σ_{L_1} and σ_{L_2}. However, the ionization cross sections for L_3 and total (see Table II) are in good agreement (within 6.0% on

TABLE II. Total L-shell ionization cross section σ_{L_T} of Pb and Bi for α-particle bombardment.

α-particle energy (MeV/amu)	σ_{L_T} of Pb (barn)			σ_{L_T} of Bi (barn)		
	Theory	Expt. using decay yields		Theory	Expt. using decay yields	
	ECPSSR	Krause	Xu and Xu	ECPSSR	Krause	Xu and Xu
0.571	7.29	7.22	7.41	6.25	6.60	6.37
0.757	18.6	19.5	20.1	16.1	15.1	14.5
0.937	35.3	39.9	41.2	30.8	30.6	29.2
1.124	58.7	64.6	66.7	51.5	53.0	50.5
1.306	87.3	96.5	99.7	76.7	73.2	69.7
1.492	122	135	140	108	111	108
1.675	162	179	185	143	159	151
1.863	209	230	237	185	203	193
2.046	261	286	296	230	255	243

average) with the theory [12,13]. In a previous work by Chang, Morgan, and Blatt [4]. The ionization cross section for L_2-subshell ionization for α-particle bombardment was shown to be in good agreement with the PWBA theory [7] but our present study shows large deviations from the ECPSSR result [13] in the entire projectile-energy range. However, the discrepancies found in our present results for σ_{L_1} and σ_{L_2} are consistent with the heavy-ion data of Sarkadi and Mukoyama [8]. In Figs. 3 and 4 we have shown two sets of measured ionization cross sections corresponding to two different sets of decay yield data by Krause [18] and Xu and Xu [11]. As can be seen from the figures the decay yield data of Krause [18] gives a better agreement with theory for L_1 and L_3 subshell ionization cross sections whereas the decay yield data of Xu and Xu [11] gives better agreement with theory for σ_{L_2}. Further comparison with theory is done by plotting the ionization cross section ratios $\sigma_{L_1}/\sigma_{L_2}$ and $\sigma_{L_3}/\sigma_{L_2}$ in Figs. 5 and 6. The measured ratios show large deviations from the ECPSSR theory, and especially at low projectile energy the discrepancy is quite large. For both Pb and Bi the measured ratio $\sigma_{L_1}/\sigma_{L_2}$ is found to be lower as compared to the theoretical value, and the position of the dip of the experimental curve is shifted to the left of the theoretical dip. Such a shift was also seen in previous works [4,5]. The theoretical results for the $\sigma_{L_3}/\sigma_{L_2}$ ratios (Fig. 6) of both Pb and Bi again show large discrepancies from the experimental results. Previous measurements by Li, Clark, and Greenlees [5] showed a drop in the $\sigma_{L_3}/\sigma_{L_2}$ ratio at low projectile energy (below 1 MeV/amu) for all high Z elements, but in our present study we do not see such a drop. At the same time we also do not see any rising trend as predicted by theory and as observed in the case of ionization by protons [2]. Our present results of the $\sigma_{L_3}/\sigma_{L_2}$ ratio are closer to the results of Chang, Morgan, and Blatt [3], who also did not see any drop for the elements with closed $6s$ configuration. Both Pb and Bi have closed $6s$ configuration. The kind of drop seen by Li, Clark, and

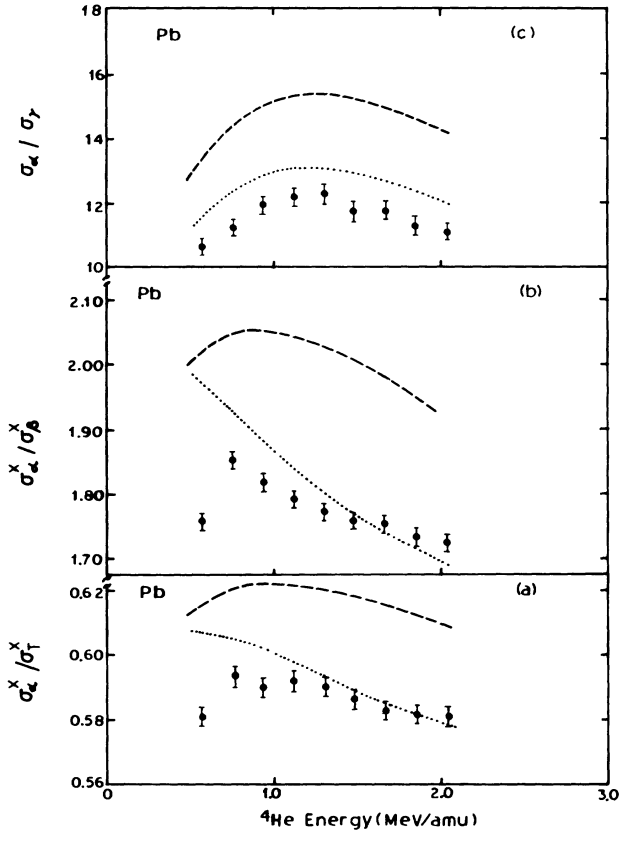

FIG. 7. Various ratios of x-ray production cross sections of Pb for α-particle bombardment: (a) $\sigma_\alpha^x/\sigma_T^x$, (b) $\sigma_\alpha^x/\sigma_\beta^x$, and (c) $\sigma_\alpha^x/\sigma_\gamma^x$: (●) corresponds to the present experimental results and (Δ) corresponds to the experimental results of Braziewicz *et al.* [6]. (· · · ·) corresponds to results obtained by using the ECPSSR ionization cross sections and decay yield data of Xu and Xu. (— — —) corresponds to results obtained by using the ECPSSR ionization cross sections and decay yield data of Krause.

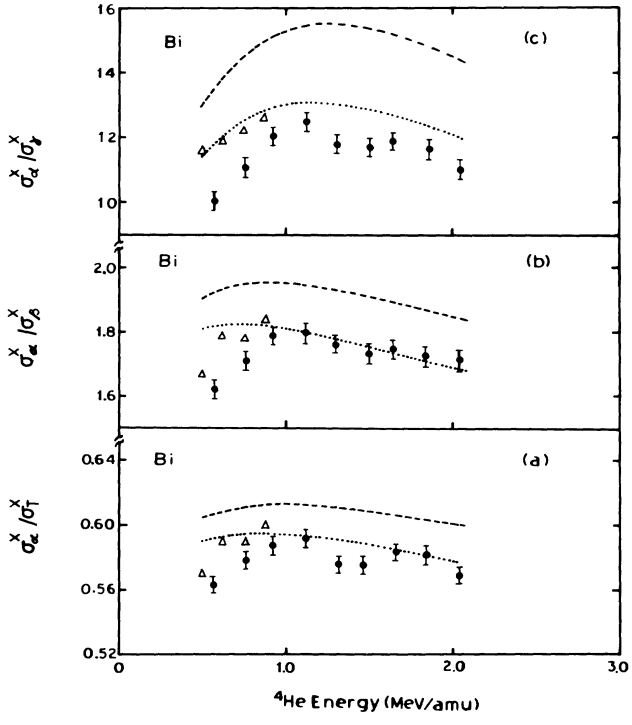

FIG. 8. Various ratios of x-ray production cross sections of Bi for α-particle bombardment: (a) $\sigma_\alpha^x/\sigma_T^x$, (b) $\sigma_\alpha^x/\sigma_\beta^x$, (c) $\sigma_\alpha^x/\sigma_\gamma^x$. (●) corresponds to present experimental results and (△) corresponds to the experimental results of Braziewicz *et al.* [6]. (· · · ·) corresponds to results obtained by using ECPSSR ionization cross sections and decay yield data of Xu and Xu. (— — —) corresponds to the results obtained by using the ECPSSR ionization cross sections and decay yield data of Krause.

Greenlees [5] for all elements irrespective of the outer electronic configuration of the target atom has not been confirmed by our present results.

The measured x-ray production cross section ratios of Pb and Bi are compared with the theoretical results in Figs. 7 and 8. In Fig. 8 we have also plotted the bismuth results of Braziewicz *et al.* [6]. the results of Refs. [14,15] and the recent results of Semaniak *et al.* [16] could not be plotted because of the lack of tabulated data. Although the theoretical results calculated using the decay yield data of Xu and Xu [11] agree better with the experimental results, one should not take this agreement very seriously because it may so happen that the x-ray production cross sections (Figs. 9 and 10) are not in good agreement but the ratio of individual production cross sections is good. Evidence in favor of this argument can be seen in comparison to total x-ray production cross sections shown in Figs. 9 and 10. The results of Braziewicz *et al.* [6] for the relative x-ray production cross sections of Bi are somewhat higher as compared to our present results and agreed better with the results of Xu and Xu results [11], but their total production cross sections are not in as good agreement with theory as ours [see Fig. 10].

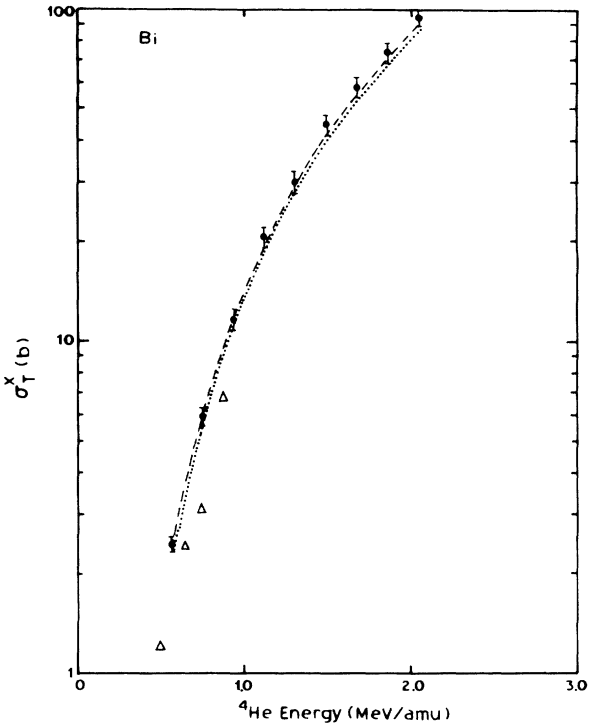

FIG. 10. Total x-ray production cross section of Bi for α-particle bombardment in the energy range 0.57–2.2 MeV/amu. (●) corresponds to present experimental data; (— — —) corresponds to results obtained from the ECPSSR ionization cross sections and decay yield data of Krause; (· · · ·) corresponds to results obtained from ECPSSR ionization cross sections and decay yield data of Xu and Xu.

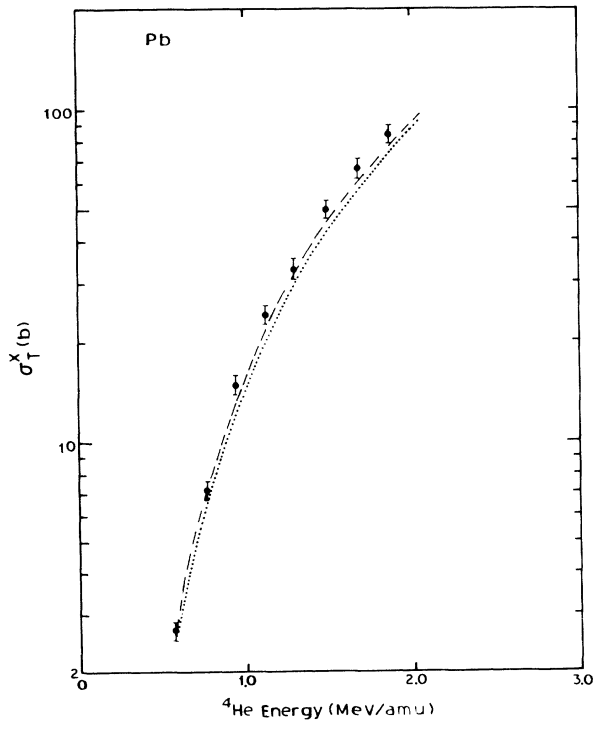

FIG. 9. Total x-ray production cross sections of Pb for α-particle bombardment in the energy range 0.57–2.2 MeV/amu. (●) corresponds to present experimental data; (— — —) corresponds to results obtained from the ECPSSR ionization cross sections and decay yield data of Krause; (· · · ·) corresponds to results obtained from the ECPSSR ionization cross sections and decay yield data of Xu and Xu.

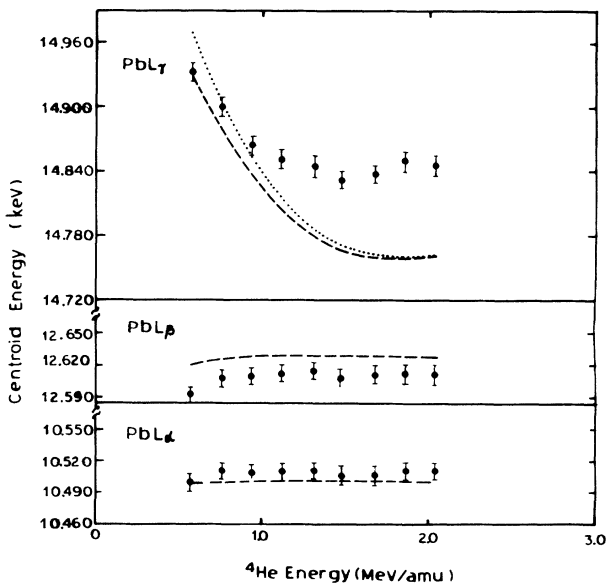

FIG. 11. Centroid energies of various L x-ray lines of Pb. (●) corresponds to present experimental points; (· · · ·) corresponds to results obtained from the ECPSSR theory and decay yield data of Xu and Xu; (— — —) corresponds to results obtained from the ECPSSR theory and decay yield data of Krause. For $L\alpha$ and $L\beta$ centroid energies, the theoretical results obtained for Xu and Xu and Krause are same.

The experimental centroid energies of the composite L x-ray peaks are estimated as given in the reference of Bissinger *et al.* [20] and compared with the theoretical calculations in Figs. 11 and 12. Since the $L\alpha$ transition involves only the L_3 subshell, no shift of the centroid energy is expected for this line with projectile energy unless there is any multivacancy formation and none is observed. Relative variation in the L-subshell hole production is expected to produce a beam-energy-dependent shift in the centroid positions of the $L\beta$ and $L\gamma$ lines which are composite lines with contributions from at least two subshells. Variation of the $L\beta$ centroid energy with α-particle energy is well explained by the ECPSSR theory [12,13] for both Pb and Bi. However, in the case of $L\gamma$ centroid energy, we find some discrepancy between theory and experiment. Moreover, the discrepancy in the case of Pb is at the low projectile energy and for Bi it is at the high energy side. The reason for this difference is not quite clear to us. It may be because of the fact that the hole-subshell cross-section-ratio variation with bombarding energy predicted by the theory is not correct for different parts of the projectile energy range in Pb and Bi.

In summary, we would like to say that the present study on L-subshell ionization in Pb and Bi by α particles has revealed some new features of the ionization process. The ECPSSR theory is found to be inadequate in explaining the measured L_1- and L_2-subshell ionization cross sections. Calculations taking into account the collision-induced intrashell transition effects are needed in order to remove the present discrepancy between theory and experiment.

We also feel that the problem of the dependence of α-particle-induced L-shell ionization on an outer electron configuration of the target atom is not yet fully settled. Although the work of Li, Clark, and Greenlees [5] has ruled out this dependence, our present study keeps the problem alive again and it is necessary to carry out a systematic study on many targets with filled and unfilled $6s$ states in order to get a clearer picture of the problem. In order to check this point our next plan will be to carry out fresh measurements in some more elements with the atomic number in the region $70 < Z < 94$.

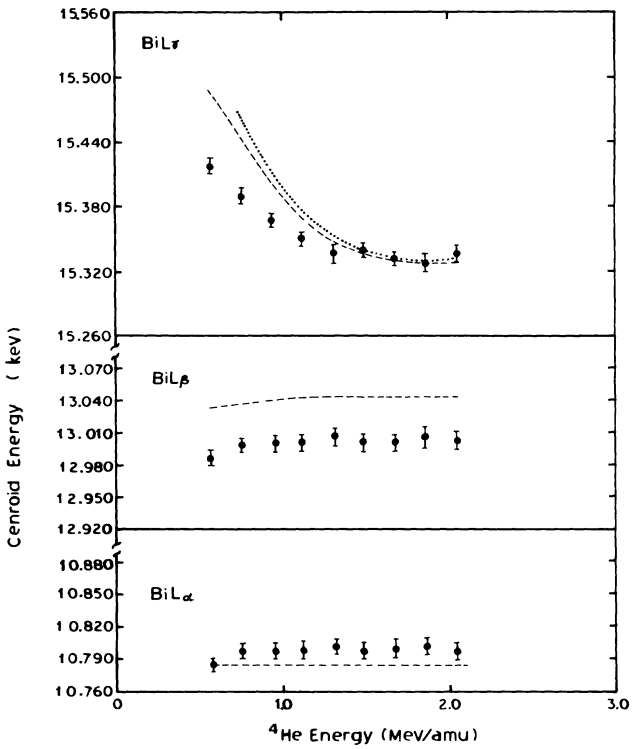

FIG. 12. Centroid energies of various L x-ray lines of Bi. (●) corresponds to present experimental points; (· · · ·) corresponds to results obtained from the ECPSSR theory and decay yield data of Xu and Xu; (— — —) corresponds to the results obtained from the ECPSSR theory and decay yield data of Krause. For $L\alpha$ and $L\beta$ centroid energies, the theoretical results obtained for Xu and Xu and Krause are same.

[1] H. C. Padhi, C. R. Bhuinya, B. B. Dhal, and S. Mishra (unpublished).
[2] S. Datz, J. L. Duggan, L. C. Feldman, E. Laegsgaard, and J. U. Anderson, Phys. Rev. A **9**, 192 (1974).
[3] C. N. Chang, J. F. Morgan, and S. L. Blatt, Phys. Lett. **49A**, 365 (1974).
[4] C. N. Chang, J. F. Morgan, and S. L. Blatt, Phys. Rev. A **11**, 607 (1975).
[5] T. K. Li, D. L. Clark, and G. W. Greenlees, Phys. Rev. Lett. **37**, 1209 (1976).
[6] J. Braziewicz, E. Braziewicz, J. Ploskonika, M. Pajek, and G. M. Osetynski, J. Phys. B **17**, 3245 (1984).
[7] B. H. Choi, E. Merzbacher, and G. S. Khandelwal, At. Data **5**, 291 (1973).
[8] L. Sarkadi and T. Mukoyama, J. Phys. B **13**, 2255 (1980).
[9] L. Sarkadi and T. Mukoyama, J. Phys. B **14**, L255 (1981).
[10] L. Sarkadi and T. Mukoyama, Phys. Rev. A **37**, 4540 (1988).
[11] J. Q. Xu and X. J. Xu, J. Phys. B **25**, 695 (1992).
[12] W. Brandt and G. Lapicki, Phys. Rev. A **23**, 1717 (1981).
[13] D. D. Cohen and M. Harrigan, At. Data Nucl. Data Tables **33**, 255 (1985).
[14] P. Komarek, Acta. Phys. Aust. **27**, 369 (1968).
[15] S. T. Thornton, R. H. McKnight, and R. R. Karlowitz, Phys. Rev. A **10**, 219 (1974).
[16] J. Semaniak, J. Braziewicz, M. Pajek, A. P. Kobzev, and D. Trautmann, Nucl. Instrum. Methods Phys. Res. B **75**, 63 (1993).
[17] J. H. Hubbell, W. H. McMaster, N. K. Del Grande, and J. H. Hammellet, in *International Tables for X-Ray Crystallography*, edited by J. A. Ibers and J. C. Hamilton (Keynoch, Birmingham, 1974), Vol. 4, p. 47.
[18] M. O. Krause, J. Phys. Chem. Ref. Data **8**, 307 (1979).
[19] J. H. Scofield, Phys. Rev. A **10**, 1507 (1974).
[20] G. A. Bissinger, A. B. Baskin, B. H. Choi, S. M. Safroth, J. M. Howard, and A. W. Waltner, Phys. Rev. A **6**, 545 (1972).